

## Electron doubly differential cross section for 0.5-MeV $H^-$ -He detachment collisions

Chang-Hwan Park, Anthony F. Starace, and Joseph Macek

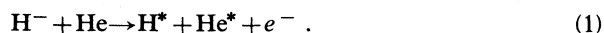
*Department of Physics and Astronomy, The University of Nebraska, Lincoln, Nebraska 68588-0111*

(Received 16 October 1984)

A comprehensive theoretical treatment is presented for the electron detachment cross section, differential in both electron momentum and direction, for collisions of 0.5-MeV  $H^-$  projectiles on He targets. Our calculation, which assumes that the residual H atom is left in the  $1s$  state, employs the usual first Born approximation as well as the closure approximation (in order to sum over all He target final states). Electron correlations within the  $H^-$  system are treated in detail within the framework of the adiabatic hyperspherical coordinate approximation. In particular, for the first time for this collision process, angular correlations are included. The  $s$ ,  $p$ , and  $d$  partial-wave components of the detached electron hyperspherical coordinate wave function are also included. The helium target is described by the atomic form factor and the incoherent scattering function tabulated by Hubbell *et al.* as well as by an average He excitation energy,  $\bar{I}_{He}$ . The prescription of Lee and Chen for  $\bar{I}_{He}$ , which for small scattering angles gives the value 35 eV is found to result in the best agreement of our calculated doubly differential cross sections with experiment, both in shape and in predicted peak energies. The unique feature of the experimental doubly differential detachment cross section of Menendez and Duncan, that for electron-scattering angles less than  $4^\circ$  there is a double peak, is reproduced in our calculations. However, the predicted higher-energy peak is smaller in magnitude and higher in energy than that observed experimentally. This difference is attributed to the influence of excited H-atom states, which are measured in the experiments. Fictitious calculations are carried out for the doubly differential cross sections in which the  $s$ -wave electron phase shift is fixed at zero radians instead of its true monotonically decreasing value with increasing electron energy from the value  $\pi$  at threshold. These fictitious calculations demonstrate the disappearance of the double-peak structure of the cross section and confirm the origin of the double peak in the  $s$ - and  $p$ -wave interference and in the initial  $\pi$  phase shift of the  $s$  partial wave. Though our single differential cross sections differ quantitatively from previous calculations of Maleki and Macek, the approximate factor of 2 discrepancy between the theoretical predictions and the absolute experimental measurements remains unexplained.

### I. INTRODUCTION

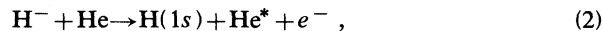
Electron doubly differential cross sections provide much more detailed information on ion-atom collision dynamics than do total cross sections for electron production.<sup>1,2</sup> Until recently, however, nearly all theoretical and experimental work on detachment collisions of negative ions with neutral atoms focused on the energy dependence of the total electron production cross section. This work has been surveyed by Risley.<sup>3</sup> In recent years, however, Menendez and Duncan<sup>4-6</sup> have studied experimentally the doubly differential collisional electron detachment cross section of  $H^-$  by He, primarily at an incident ion velocity of 0.5 MeV. More specifically, they measured the energy distribution of the detached electrons at several fixed laboratory angles for the following process:



The asterisks on the right in Eq. (1) indicate that the corresponding atoms may be either in an excited state, bound or continuum, or in the unexcited ground state. The experiment does not distinguish among these cases. A key feature of the experimental data is that for electrons detached at angles close to  $0^\circ$  in the laboratory frame, the intensity distribution of electrons, as a function of electron

kinetic energy, has *two* peaks, separated by about 30 eV, instead of the more usual single peak predicted by the binary encounter theory.<sup>2</sup> The observed higher-energy peak, which occurs at an electron velocity equal to the incident  $H^-$  velocity, decreases in intensity with increasing laboratory-frame scattering angle, and it disappears altogether for angles greater than about  $4^\circ$ .

This experimental work has led to a number of theoretical studies<sup>7-10</sup> for the dominant process in Eq. (1), i.e.,



in which the hydrogen atom is not excited during the collision. Qualitatively, the main features of the experimental data are now understood theoretically. In particular, the double-peak structure seen experimentally has been shown to arise theoretically from an interference of  $s$  and  $p$  partial waves for the detached electron.<sup>7</sup> This interference is most visible in the projectile-frame doubly differential cross section.<sup>9</sup> A recent study has shown both experimentally and theoretically that this interference is more significant the larger the mean excitation energy of the target atom or molecule,<sup>5</sup> thereby explaining why it is particularly apparent for He targets. However, quantitative agreement between theory and experiment is poor: The energy positions of the observed peaks and their rela-

tive magnitudes are not well predicted theoretically.

The poor quantitative agreement between theory and experiment has several probable causes. First, all such theoretical calculations are very sensitive to electron correlations in the  $H+e^-$  system, particularly for the small projectile-frame electron energies at which the  $s$  and  $p$  partial-wave interference effects are most significant. Moreover, the theoretical calculations carried out to date have treated the  $H+e^-$  system very approximately. In particular, they all focus exclusively on treating only radial correlations and not angular correlations.

Second, all of the theoretical calculations treat the summation over the final states of the He target approximately. They are thus subject to any inaccuracies in the calculation of the He form factors. More important, however, given the demonstrated<sup>5</sup> sensitivity of the detachment collision process to the target's mean excitation energy, is the choice of this mean excitation energy.

Finally, both experimental<sup>6,11</sup> and theoretical<sup>12</sup> evidence points to the importance of excited states of the hydrogen atom to the experimental doubly differential cross sections measured for the process in Eq. (1). Experimentally, it has long been known<sup>11</sup> that  $n=2$  states of the residual H atom are important contributors to the total detachment cross section for the process in Eq. (1). Recently, both theory<sup>12</sup> and experiment<sup>6</sup> have indicated the likelihood that excited states of the H atom are important contributors to the higher-energy peak seen in the doubly differential detachment cross section. However, without an accurate calculation for the dominant process, given in Eq. (2), it is not clear what fraction of the high-energy peak should be attributed to states in which the H atom is unexcited and what fraction should be attributed to states involving excited H atoms.

The present paper presents a comprehensive calculation of the dominant detachment process in Eq. (2) for an incident projectile energy of 0.5 MeV. Calculations of the doubly differential detachment cross sections are carried out using the first Born approximation and including  $s$ ,  $p$ , and  $d$  partial waves for the detached electron. Both radial and angular correlations are treated for the  $H+e^-$  system through our use of adiabatic hyperspherical coordinate wave functions.<sup>13</sup> [Thus, for example, our hyperspherical coordinate wave function for the  $H^-$  ground state incorporates angular correlations of the form  $ss$ ,  $pp$ ,  $dd$ , and  $ff$ ; our calculated  $H^-$  ground-state energy is  $-0.52592$  a.u. (upper bound) as compared to the "exact" result<sup>14</sup> of  $-0.527751$  a.u.] Similarly, wave functions for the  $^1S$ ,  $^1P$ , and  $^1D$  final states are calculated also in the adiabatic hyperspherical approximation.<sup>13</sup>

To sum over the final states of the He target we have employed the usual closure approximation.<sup>15</sup> We have used the form factor and incoherent scattering function for He as tabulated by Hubbell *et al.*<sup>16</sup> Our calculations have been carried out using two prescriptions<sup>15,17</sup> for the average excitation energy of He. We find that the prescription of Lee and Chen,<sup>17</sup> involving an average momentum transfer for small-angle scattering, provides the best agreement with the experimental data.<sup>4-6</sup>

Our aim is thus to present quantitatively accurate predictions for the dominant detachment process in Eq. (2)

for comparison with the experimental data<sup>4-6</sup> for the detachment process in Eq. (1). Differences between our results and experiment thereby serve to indicate the magnitude of contributions from excited states of H to the process in Eq. (1).

In Sec. II we review the theoretical formulation of the doubly differential detachment cross section in the first Born approximation. In Sec. III we discuss the further approximations and some numerical details of the present calculation, in particular the calculation of the  $H^-$  form factor in hyperspherical coordinates. Our results for the doubly differential detachment cross section are presented in Sec. IV and compared with experiment as well as with previous theoretical calculations. Finally, we summarize our findings and conclusions in Sec. V.

## II. FIRST BORN APPROXIMATION FORMULA FOR THE DETACHMENT CROSS SECTION

The doubly differential cross section for electron detachment following collision of a projectile ion ( $H^-$ ) with a target atom (He) is given in the first Born approximation by<sup>9,18</sup>

$$\left. \frac{d\sigma}{d\omega dE} \right|_{if} = \frac{k}{4\pi^2 v_i^2} \int_0^{2\pi} \int_{K_{\min}}^{K_{\max}} |\langle \Psi_f | V | \Psi_i \rangle|^2 K dK d\phi. \quad (3)$$

Here  $k$  is the momentum,  $d\omega$  is the solid angle, and  $E$  is the energy of the detached electron;  $v_i$  is the relative velocity of the projectile with respect to the target ( $v_i = 4.47135$  a.u. for 0.5-MeV  $H^-$  incident on He);  $\mathbf{K}$  is the momentum transfer,

$$\mathbf{K} \equiv \mathbf{k}_i - \mathbf{k}_f, \quad (4)$$

where  $\mathbf{k}_i$  and  $\mathbf{k}_f$  are the initial and final momenta of the projectile;  $\phi$  is the azimuthal angle of the scattered projectile;  $K_{\max}$  and  $K_{\min}$  are the maximum and minimum magnitudes for the momentum transfer;  $V$  is the electrostatic interaction potential between the projectile and target; and  $\Psi_f$  and  $\Psi_i$  are the final- and initial-system wave functions. Atomic units are used throughout this paper.

We have computed Eq. (3) in the projectile frame, which is most convenient theoretically for computation of the detached electron wave function. In this frame the target (He) has an initial relative velocity of  $-\mathbf{v}_i$  and initial and final momenta of  $-\mathbf{k}_i$  and  $-\mathbf{k}_f$ , respectively. To compare our results with experiment, we must transform projectile-frame cross sections to the laboratory frame. To do this we note that under any Galilean transformation,  $d\sigma$  is invariant, as is

$$d\mathbf{k} = dk_x dk_y dk_z = k^2 dk d\omega = k dE d\omega. \quad (5)$$

Comparison of Eq. (5) with Eq. (3) shows that  $k^{-1}(d\sigma/d\omega dE)$  is Galilean invariant.<sup>9</sup> The desired laboratory-frame doubly differential cross section is thus obtained by multiplying the projectile-frame doubly differential cross section by the factor  $(k_L/k_P)$ , i.e., the ratio of the detached electron momenta in the laboratory ( $L$ ) and projectile ( $P$ ) frames, respectively.

In the Born approximation each of the initial- and final-system wave functions  $\Psi_i$  and  $\Psi_f$  consists of a triple product of a plane-wave wave function, describing the relative motion of the projectile and target nuclei, and electronic wave functions describing the states of the projectile and target systems. Since  $H^-$  and He are each two-electron systems,  $\Psi_i$  and  $\Psi_f$  are functions of fifteen coordinates: twelve to describe the motion of the four electrons and three to describe the relative nuclear motion. In computing the matrix element of the electrostatic potential  $V$  among the nuclei and electrons, use is made of a theorem of Bethe<sup>19,20</sup> to integrate over the relative nuclear coordinates. The remaining integrations over the electronic coordinates are described by the transition form factors for the  $H^-$  and He systems.

The final result for the electrostatic matrix element between the system wave functions  $\Psi_{00}$  and  $\Psi_{nk}^-$  where 00 indicates that initially both  $H^-$  and He are in their ground states and where  $nk$  indicates that in the final state the He atom is excited to the state  $n$  and the  $H^-$  ion has been ionized leaving the atom in its ground state 1s and the detached electron with momentum  $\mathbf{k}$ , is

$$\langle \Psi_{nk}^- | V | \Psi_{00} \rangle = \frac{4\pi}{K^2} \epsilon_{0k}^{H^-}(\mathbf{K}) [\epsilon_{0n}^{He}(\mathbf{K}) - 2\delta_{0n}]. \quad (6)$$

$$\frac{d\sigma}{d\omega dE} = \sum_{n=0}^{\infty} \frac{4k}{v_i^2} \int_0^{2\pi} d\phi_{He} \int_{K_{\min}^{(n)}}^{K_{\max}^{(n)}} dK |\epsilon_{0k}^{H^-}(\mathbf{K})|^2 |\epsilon_{0n}^{He}(\mathbf{K}) - 2\delta_{0n}|^2 \frac{1}{K^3}. \quad (9)$$

In Eq. (9) the sum over  $n$  implies also integration over singly and doubly ionized continuum states. Furthermore, the index  $n$  on the limits of integration over the magnitude of the momentum transfer indicates that these limits are dependent on the final state of the target, as is clear from the definition in Eq. (4).

### III. FURTHER THEORETICAL APPROXIMATIONS

The Born approximation result in Eq. (9) requires for its numerical evaluation additional approximations in order to sum over all final states of the He target and in order to calculate the transition form factors for He and for  $H^-$ . We examine each of these necessary approximations in turn.

#### A. Closure approximation

If we ignore the dependence of the integration limits in Eq. (9) on the final state  $n$ , having wave function  $\phi_n$ , of the He target, then the following closure relation may be employed to sum the absolute square of Eq. (8) over final states  $n$ :

$$\sum_{n>0} |\phi_n\rangle \langle \phi_n| = 1 - |0\rangle \langle 0|. \quad (10)$$

The result is

In Eq. (6) the minus superscript on the final-state wave function indicates that incoming wave boundary conditions are used.<sup>21</sup> The term  $-2$  in the square brackets arises from interaction of the  $H^-$  electrons with the  $He^{2+}$  nucleus. This interaction contributes to the transition matrix element only when the He target is unexcited during the collision, i.e., when  $n=0$ , as indicated by the Kronecker  $\delta$  function. The transition form factors are defined as follows:

$$\epsilon_{0k}^{H^-}(\mathbf{K}) \equiv \left\langle \psi_{\mathbf{k}}^- \left| \sum_{i=1}^2 \exp(i\mathbf{K} \cdot \mathbf{r}_i) \right| \psi_0 \right\rangle, \quad (7)$$

$$\epsilon_{0n}^{He}(\mathbf{K}) \equiv \left\langle \phi_n \left| \sum_{i=1}^2 \exp(-i\mathbf{K} \cdot \boldsymbol{\rho}_i) \right| \phi_0 \right\rangle. \quad (8)$$

In Eq. (7),  $\psi_0(\mathbf{r}_1, \mathbf{r}_2)$  and  $\psi_{\mathbf{k}}^-(\mathbf{r}_1, \mathbf{r}_2)$  describe the initial and final  $H^-$  states as functions of the electronic coordinates  $\mathbf{r}_1$  and  $\mathbf{r}_2$ . Similarly,  $\phi_0(\boldsymbol{\rho}_1, \boldsymbol{\rho}_2)$  and  $\phi_n(\boldsymbol{\rho}_1, \boldsymbol{\rho}_2)$  in Eq. (8) describe the initial and final He states as functions of the electronic coordinates  $\boldsymbol{\rho}_1$  and  $\boldsymbol{\rho}_2$ .

The Born approximation result for the doubly differential cross section for the detachment process in Eq. (2) is obtained by substituting Eq. (6) in Eq. (3) and summing over all final states of the He target:

$$\sum_{n>0} |\epsilon_{0n}^{He}(\mathbf{K})|^2 = \sum_{i,j=1}^2 \langle \phi_0 | e^{i\mathbf{K} \cdot (\boldsymbol{\rho}_i - \boldsymbol{\rho}_j)} | \phi_0 \rangle - \left| \left\langle \phi_0 \left| \sum_{i=1}^2 e^{i\mathbf{K} \cdot \boldsymbol{\rho}_i} \right| \phi_0 \right\rangle \right|^2 \quad (11a)$$

$$\equiv S_{\text{inc}}(K), \quad (11b)$$

where  $S_{\text{inc}}(K)$  is the incoherent scattering function, which is dependent only on the magnitude  $K$  of the momentum transfer since it is defined in terms of ground-state expectation values. Substituting Eq. (11) in Eq. (9), we obtain

$$\frac{d\sigma(k, \theta)}{d\omega dE} = \frac{8\pi k}{v_i^2} \int_{K_{\min}^{(0)}}^{K_{\max}^{(0)}} J(K, \mathbf{k}) |\epsilon_{00}^{He}(K) - 2|^2 \frac{dK}{K^3} + \frac{8\pi k}{v_i^2} \int_{K_{\min}^{(\bar{I}_{He})}}^{K_{\max}^{(\bar{I}_{He})}} J(K, \mathbf{k}) S_{\text{inc}}^{He}(K) \frac{dK}{K^3}. \quad (12)$$

Here the index 0 on the limits of integration in the first integral indicates that  $K_{\min}^{(0)}$  and  $K_{\max}^{(0)}$  are appropriate for the case in which the He target remains unexcited, while the index  $\bar{I}_{He}$  in the second integral implies that  $K_{\min}^{(\bar{I}_{He})}$  and  $K_{\max}^{(\bar{I}_{He})}$  are calculated for some average excitation state of the He target having excitation energy  $\bar{I}_{He}$ . The function  $J(K, \mathbf{k})$  is defined by

$$J(K, \mathbf{k}) = \frac{1}{2\pi} \int_0^{2\pi} |\epsilon_{0k}^{H^-}(\mathbf{K})|^2 d\phi_f. \quad (13)$$

It is thus an average of the absolute square of the  $H^-$  transition form factor over all azimuthal scattering angles  $\phi_f$  of the He target [N.B., in the projectile (i.e.,  $H^-$ ) frame the He target is the scattered particle]. Because of the averaging over the azimuthal scattering angle,  $J(K, \mathbf{k})$  is a function of the magnitude  $K$  of the momentum transfer as well as the momentum  $k$  and scattering angle  $\theta$  of the detached electron. In our calculations we have employed the atomic form factor  $\epsilon_{00}^{\text{He}}(K)$  and the incoherent scattering function  $S_{\text{inc}}^{\text{He}}(K)$  that have been tabulated by Hubbell *et al.*<sup>16</sup>

### B. Integration limits

By definition, the maximum and minimum values of the momentum transfer needed to carry out the integration in Eq. (12) are

$$K_{\text{max}} = k_f + k_i, \quad (14a)$$

$$K_{\text{min}} = k_i - k_f, \quad (14b)$$

where

$$k_i = \mu v_i. \quad (14c)$$

Here  $k_i$  and  $k_f$  are the initial and final momentum vectors for the projectile and  $\mu$  is the reduced mass of the projectile and target system. Because of the large momentum of the incident 0.5-MeV  $H^-$  projectile, we may, independently of the excitation state of the He target, approximate the upper limit as follows:

$$K_{\text{max}} \approx 2k_i = 2\mu v_i = 1.31299 \times 10^4 \text{ a.u.} \quad (15)$$

The lower limit requires more careful consideration. We write it in terms of the initial and final kinetic energy of the projectile,  $E_{i,f} \equiv k_{i,f}^2/2\mu$ , as follows:

$$K_{\text{min}} = \frac{k_i^2 - k_f^2}{k_i + k_f} \approx \frac{(k_i^2 - k_f^2)/\mu}{2k_i/\mu} = \frac{E_i - E_f}{v_i}. \quad (16)$$

Now by energy conservation, we may equate the initial- and final-system energies in the projectile frame to obtain the following results for  $E_i - E_f$  and hence for  $K_{\text{min}}$ :

$$K_{\text{min}}(0) = \frac{I_{H^-} + k^2/2}{v_i} \quad (17a)$$

for no target excitation and

$$K_{\text{min}}(\bar{I}_{\text{He}}) = \frac{I_{H^-} + \bar{I}_{\text{He}} + k^2/2}{v_i} \quad (17b)$$

for the case of an average target excitation  $\bar{I}_{\text{He}}$ .

In our calculations  $I_{H^-}$  is 0.027751 a.u. and two alternative values of  $\bar{I}_{\text{He}}$  are used. One common alternative is to set  $\bar{I}_{\text{He}}$  equal to the energy necessary to excite the lowest excited state of the target.<sup>15</sup> For He this is the  $1s2s(^3S)$  state. We have chosen instead to set one of our alternative  $\bar{I}_{\text{He}}$  values equal to 0.77975 a.u., corresponding to the  $1s2p(^1P)$  state. Lee and Chen<sup>17</sup> have described another alternative: They calculate an angle-dependent, average momentum transfer and excitation energy. For the small projectile scattering angles significant here,  $\bar{I}_{\text{He}}$  is approximately 35 eV or 1.28625 a.u.<sup>12</sup> We have chosen this value as the second of our two alternative  $\bar{I}_{\text{He}}$  values.

### C. $H^-$ wave functions

The  $H^-$  transition form factor in Eq. (7) is very sensitive to the form of the initial- and final-state wave functions used.<sup>9</sup> We treat the important electron correlations involved by means of an adiabatic hyperspherical coordinate representation.<sup>13</sup> The exact two-electron wave function  $\psi(\mathbf{r}_1, \mathbf{r}_2)$  may be expanded in terms of a complete set of adiabatic eigenfunctions  $\phi_\mu(R, \alpha, \hat{\mathbf{r}}_1, \hat{\mathbf{r}}_2)$ , which depend parametrically on the hyperspherical radius  $R \equiv (r_1^2 + r_2^2)^{1/2}$  and are functions of the five angular variables  $\alpha \equiv \tan^{-1}(r_2/r_1)$ ,  $\hat{\mathbf{r}}_1$ , and  $\hat{\mathbf{r}}_2$ . The form of  $\psi$  is thus

$$\psi(R, \alpha, \hat{\mathbf{r}}_1, \hat{\mathbf{r}}_2) = (R^{5/2} \sin \alpha \cos \alpha)^{-1} \sum_{\mu} F_{\mu}(R) \phi_{\mu}(R, \alpha, \hat{\mathbf{r}}_1, \hat{\mathbf{r}}_2). \quad (18)$$

The angular function  $\phi$  is defined to satisfy the following differential equation in atomic units ( $\hbar = e = m = 1$ ):

$$\left[ \frac{d^2}{d\alpha^2} - \frac{L_1^2}{\cos^2 \alpha} - \frac{L_2^2}{\sin^2 \alpha} + 2R \left[ \frac{Z}{\cos \alpha} + \frac{Z}{\sin \alpha} - (1 - \sin 2\alpha \cos \theta_{12})^{-1/2} \right] \right] \phi_{\mu} = U_{\mu}(R) \phi_{\mu}. \quad (19)$$

Here  $L_i^2$  is the squared orbital angular momentum operator for the  $i$ th electron,  $\theta_{12} \equiv \cos^{-1} \hat{\mathbf{r}}_1 \cdot \hat{\mathbf{r}}_2$ ,  $Z$  is the nuclear charge, and  $U_{\mu}(R)$  is the eigenvalue, which is parametrically dependent on  $R$ . The solution of Eq. (19) is carried out<sup>13</sup> by expanding the angle functions in one-electron spherical harmonics,

$$\phi_{\mu} = \sum_{l_1, l_2} g_{l_1, l_2}^{\mu}(R, \alpha) \mathcal{Y}_{l_1, l_2, LM}(\hat{\mathbf{r}}_1, \hat{\mathbf{r}}_2), \quad (20a)$$

where

$$\mathcal{Y}_{l_1, l_2, LM}(\hat{\mathbf{r}}_1, \hat{\mathbf{r}}_2) \equiv \sum_{m_1, m_2} Y_{l_1, m_1}(\hat{\mathbf{r}}_1) Y_{l_2, m_2}(\hat{\mathbf{r}}_2) (l_1 m_1 l_2 m_2 | l_1 l_2 LM), \quad (20b)$$

and then solving the resulting set of coupled differential equations [after suitable truncation of the number of angular momentum pairs  $(l_1 l_2)$ ] for the functions  $g_{l_1, l_2}^{\mu}(R, \alpha)$ . Upon substituting Eq. (18) in the two-electron Schrödinger equation and using Eq. (19), one obtains the following set of coupled differential equations for the radial functions  $F_{\mu}(R)$ :

$$\left[ \frac{d^2}{dR^2} + \frac{U_{\mu}(R) + \frac{1}{4}}{R^2} + \left[ \phi_{\mu}, \frac{\partial^2 \phi_{\mu}}{\partial R^2} \right] + 2E \right] F_{\mu}(R) + \sum_{\mu' \neq \mu} \left[ \left[ \phi_{\mu}, \frac{\partial^2 \phi_{\mu'}}{\partial R^2} \right] + 2 \left[ \phi_{\mu}, \frac{\partial \phi_{\mu'}}{\partial R} \right] \frac{\partial}{\partial R} \right] F_{\mu'}(R) = 0. \quad (21)$$

In Eq. (21) the coupling matrix elements  $(\phi_{\mu}, \partial^n \phi_{\mu'} / \partial R^n)$ ,  $n = 1, 2$ , involve integration over the five angular variables only and are thus parametrically dependent on  $R$ .

In calculating our wave functions we make an adiabatic approximation<sup>13</sup> in which we keep only a single term  $\mu$  in the summation in Eq. (18). For the ground state this term corresponds to the dominant  $1s^2(^1S)$  configuration; for the final state this term corresponds to the dominant  $1s\ell(^1L=l)$  configurations. However, this adiabatic approximation is *not* an independent particle approximation; much correlation is included. [For example, in calculating  $\phi_{\mu}$  for the initial state, using Eq. (19), an expansion of the form in Eq. (20) is made in the angular momentum pairs  $ss$ ,  $pp$ ,  $dd$ , and  $ff$ ; similar expansions are made for the final-state angle functions.] In our adiabatic approximation we include the diagonal coupling matrix element  $(\phi_{\mu}, \partial^2 \phi_{\mu} / \partial R^2)$  in solving Eq. (21) for the radial function  $F_{\mu}(R)$  but ignore all of the other off-diagonal coupling matrix elements. For the  $^1S$  ground state of  $H^-$ , this approximate solution of the eigenvalue equation, Eq. (21), may be shown<sup>22</sup> to give an upper bound on the exact system energy. Our value of  $-0.52592$  a.u. may be compared with the best variational estimate of Pekeris,<sup>14</sup> who obtains  $-0.0527751$ .

To calculate the  $H^-$  transition form factor we therefore represent the initial- and final-state wave functions as

$$\psi_0(\mathbf{r}_1, \mathbf{r}_2) = (R^{5/2} \cos\alpha \sin\alpha)^{-1} \times F_{\mu}(R) \phi_{\mu}(R, \alpha, \hat{\mathbf{r}}_1, \hat{\mathbf{r}}_2), \quad (22a)$$

$$\psi_{\mu'E}(\mathbf{r}_1, \mathbf{r}_2) = (R^{5/2} \cos\alpha \sin\alpha)^{-1} \times F_{\mu'E}(R) \phi_{\mu'}(R, \alpha, \hat{\mathbf{r}}_1, \hat{\mathbf{r}}_2). \quad (22b)$$

Note that the final-state wave function in Eq. (22b) is given in terms of the energy-normalized radial function  $F_{\mu'E}(R)$ , which satisfies the following asymptotic boundary condition:

$$F_{\mu'E}(R) \rightarrow \left[ \frac{2}{\pi k} \right]^{1/2} \sin(kr_1 - l_{\mu'}\pi/2 + \delta_{l_{\mu'}}) \quad \text{as } R \cos\alpha (=r_1) \rightarrow \infty. \quad (23)$$

Note in Eq. (23) that as the coordinate  $r_1$  of the detached electron tends toward infinity it becomes equal to the hyperradius  $R$ . Also,  $l_{\mu'}$ ,  $\delta_{l_{\mu'}}$ , and  $k$  are, respectively, the orbital angular momentum, phase shift, and momentum of the detached electron in the final-state channel  $\mu'$ . In addition, the final-state angle function  $\phi_{\mu'}$  for the channel  $\mu'$  has the asymptotic behavior<sup>13</sup>

$$\phi_{\mu'}(R, \alpha, \hat{\mathbf{r}}_1, \hat{\mathbf{r}}_2) \rightarrow r_1^{1/2} P_{1s}(r_2) Y_{00}(\hat{\mathbf{r}}_2) Y_{l_{\mu'}, m_{\mu'}}(\hat{\mathbf{r}}_1) \quad \text{as } R \cos\alpha (=r_1) \rightarrow \infty, \quad (24)$$

since we assume the H atom is not excited. Substituting Eqs. (23) and (24) in Eq. (22b) and using the relations

$r_1 = R \cos\alpha$  and  $r_2 = R \sin\alpha$ , we see that

$$\psi_{\mu'E}(\mathbf{r}_1, \mathbf{r}_2) \rightarrow \left[ \frac{2}{\pi k} \right]^{1/2} \frac{1}{r_1} \sin(kr_1 - l_{\mu'}\pi/2 + \delta_{l_{\mu'}}) \times Y_{l_{\mu'}, m_{\mu'}}(\hat{\mathbf{r}}_1) \frac{1}{r_2} P_{1s}(r_2) Y_{00}(\hat{\mathbf{r}}_2) \quad \text{as } r_1 \rightarrow \infty. \quad (25)$$

Finally, the desired incoming-wave, momentum-space normalized final-state wave function, which is needed to compute the  $H^-$  transition form factor in Eq. (7), is obtained from the standing-wave, energy-normalized wave function in Eq. (22b) as follows:<sup>21</sup>

$$\psi_{\mathbf{k}}^- = \sum_{l_{\mu'}, m_{\mu'}} (i)^{l_{\mu'}} \exp(-i\delta_{l_{\mu'}}) k^{-1/2} Y_{l_{\mu'}, m_{\mu'}}^*(\hat{\mathbf{k}}) \psi_{\mu'E}(\mathbf{r}_1, \mathbf{r}_2). \quad (26)$$

In Eq. (26) the spherical harmonic  $Y_{l_{\mu'}, m_{\mu'}}^*(\hat{\mathbf{k}})$  projects the spherical wave state  $l_{\mu'}, m_{\mu'}$  into the direction  $\hat{\mathbf{k}}$ . All spherical wave states must be summed for completeness. The two complex factors,  $(i)^{l_{\mu'}} \exp(-i\delta_{l_{\mu'}})$ , assure that the incoming wave boundary conditions are satisfied,<sup>21</sup> and the factor  $k^{-1/2}$  assures that the following orthonormality relation holds:

$$\langle \psi_{\mathbf{k}}^- | \psi_{\mathbf{k}'}^- \rangle = \delta(\mathbf{k} - \mathbf{k}'). \quad (27)$$

#### D. $H^-$ transition form factor

To calculate the  $H^-$  transition form factor in Eq. (7) we expand the plane wave in the integrand in spherical partial waves, i.e.,

$$\exp(i\mathbf{K} \cdot \mathbf{r}_i) = \sum_{l=0}^{\infty} \sum_{m=-l}^l 4\pi (i)^l j_l(Kr_i) \times Y_{lm}^*(\hat{\mathbf{K}}) Y_{lm}(\hat{\mathbf{r}}_i), \quad (28)$$

and substitute Eqs. (20), (22), and (26) for the initial and final wave functions. The result, after carrying out all angular integrations analytically, is

$$\epsilon_{0k}^{H^-}(\mathbf{K}) = \sum_{l_{\mu'}=0}^{\infty} \exp(+i\delta_{l_{\mu'}}) \times P_{l_{\mu'}}(\hat{\mathbf{K}} \cdot \hat{\mathbf{k}}) Q_{l_{\mu'}}^{l_{\mu'}}(K, k). \quad (29)$$

In Eq. (29) the  $(l_{\mu'})$ th partial-wave transition form factor,  $Q_{l_{\mu'}}^{l_{\mu'}}$  is defined by

$$Q_{l_{\mu'}}^{l_{\mu'}}(K, k) \equiv (4\pi k)^{-1/2} (2l_{\mu'} + 1) \times \int_0^{\infty} dR F_{\mu}(R) F_{\mu'E}(R) I_{l_{\mu'}}^{l_{\mu'}}(K, R), \quad (30a)$$

where  $I$ , which depends on  $R$  but not on  $k$ , is defined by

$$I_{l_{\mu'}}^{l_{\mu'}}(K, R) \equiv \sum_{l_1, l_2} (2l_2 + 1)^{1/2} \begin{pmatrix} l_2 & l_{\mu'} & l_1 \\ 0 & 0 & 0 \end{pmatrix} (-1)^{l_2} \int_0^{\pi/2} d\alpha g_{l_1 l_2}^{\mu'}(R, \alpha) [g_{l_1 l_2}^{\mu'}(R, \alpha) j_{l_1}(KR \sin\alpha) + g_{l_2 l_1}^{\mu'}(R, \alpha) j_{l_1}(KR \cos\alpha)]. \quad (30b)$$

### E. Integration over azimuthal angles

In order to compute the doubly differential cross section in Eq. (12), we must average over all projectile azimuthal scattering angles  $\phi_f$ , as in Eq. (13). From Eq. (29) we see that the dependence of the  $H^-$  transition form factor on the scattering angle  $\phi_f$ , comes from the argument of the Legendre polynomials,

$$\hat{\mathbf{K}} \cdot \hat{\mathbf{k}} \equiv \frac{\mathbf{k}_i - \mathbf{k}_f}{K} \cdot \hat{\mathbf{k}}. \quad (31a)$$

If we choose  $\hat{\mathbf{k}}_i$  to be along the  $z$  axis, then

$$\mathbf{k}_i \cdot \hat{\mathbf{k}} = k_i \cos \theta, \quad (31b)$$

$$\mathbf{k}_f \cdot \hat{\mathbf{k}} = k_f [\cos \theta_f \cos \theta + \sin \theta_f \sin \theta \cos(\phi_f - \phi)], \quad (31c)$$

where  $\theta$  and  $\phi$  define the direction of the detached electron,  $\hat{\mathbf{k}}$ , and  $\theta_f$  and  $\phi_f$  define that of the scattered projectile,  $\mathbf{k}_f$ . In our calculations we have approximated the  $H^-$  transition form factor in Eq. (29) by truncating the sum over partial-wave angular momenta  $l_{\mu'}$  for  $l_{\mu'}$  greater than 2 so that

$$\begin{aligned} \epsilon_{0k}^{H^-}(\mathbf{K}) \approx & \exp(i\delta_0) Q_{\mu\mu'}^0(K, k) + \exp(i\delta_1) (\hat{\mathbf{K}} \cdot \hat{\mathbf{k}}) Q_{\mu\mu'}^1(K, k) \\ & + \exp(i\delta_2) 0.5 [3(\hat{\mathbf{K}} \cdot \hat{\mathbf{k}})^2 - 1] Q_{\mu\mu'}^2(K, k). \end{aligned} \quad (32)$$

Substituting Eqs. (31) and (32) in Eq. (13) we obtain

$$J(K, \mathbf{k}) = \sum_{n=0}^4 (\cos^n \theta) Z_n(K, k), \quad (33)$$

where  $Z_n(K, k)$  is defined in the Appendix. Note that in averaging over  $\phi_f$  we eliminate any dependence of  $J(K, \mathbf{k})$  on  $\phi$ .

Substituting Eq. (33) in Eq. (12) we obtain finally the detachment doubly differential cross section (DDCS) in terms of a power series in  $\cos \theta$ :

$$\frac{d\sigma}{d\omega dE}(k, \theta) = \sum_{n=0}^4 (\cos^n \theta) A_n(k), \quad (34a)$$

where

$$\begin{aligned} A_n(k) \equiv & \frac{8\pi k}{v_i^2} \int_{K_{\min}^{(0)}}^{K_{\max}^{(0)}} Z_n(K, k) |\epsilon_{00}^{\text{He}}(K) - 2|^2 \frac{dK}{K^3} \\ & + \frac{8\pi k}{v_i^2} \int_{K_{\min}^{(\text{He})}}^{K_{\max}^{(\text{He})}} Z_n(K, k) S_{\text{inc}}^{\text{He}}(K) \frac{dK}{K^3}. \end{aligned} \quad (34b)$$

## IV. RESULTS

### A. Galilean-invariant doubly differential detachment cross section in the projectile frame

We present here our results for  $k^{-1}(d\sigma/d\omega dE)$  since, as discussed in Sec. II, this quantity is invariant under Galilean transformations and hence is the same in the projectile and in the laboratory frames for electron momenta  $\mathbf{k} \equiv (k, \theta)$  related by the Galilean transformation between the two reference frames.

In Table I we present the coefficients  $C_n(k)$  for the expansion of  $k^{-1}(d\sigma/d\omega dE)$  in powers  $n$  of  $\cos \theta$  in the projectile frame. The coefficients  $C_n(k)$  are simply the coefficients  $A_n(k)$  in Eq. (34a) divided by  $k$ . In our calculations we have computed these coefficients for  $0 \leq n \leq 4$  and  $0 \leq k \leq 1.0$  a.u. The restriction on the maximum value of  $n$  stems from our inclusion of only  $s$ ,  $p$ , and  $d$  partial waves in our calculation. Although we have computed coefficients  $C_n(k)$  for  $k$  values up to 1.0 a.u., we show in Table I only coefficient values for  $k \leq 0.5$  a.u. This is done because our truncation in partial waves and our use of single-channel adiabatic hyperspherical wave functions is expected to become increasingly less accurate as  $k$  increases.

In Fig. 1 we show a three-dimensional plot of the detachment DDCS in the projectile frame as a function of  $\mathbf{k} = (k, \theta)$ . Our results in Fig. 1 employ an effective exci-

TABLE I. Coefficients  $C_n(k)$  for the doubly differential, Galilean-invariant detachment cross section expressed in powers  $n$  of  $\cos \theta$ , where the detached electron has momentum  $k$  and direction  $\theta$  in the projectile frame. The coefficients  $C_n(k)$  are equal to  $k^{-1}A_n(k)$ , where the coefficients  $A_n(k)$  are defined in Eq. (34a). The integers in parentheses indicate the power of ten multiplying the preceding number.

$k$	$C_0$	$C_1$	$C_2$	$C_3$	$C_4$
0.02	+2.5280	-3.5742 (-1)	+3.0552 (-3)	+7.1711 (-3)	+9.6537 (-4)
0.06	+2.3874	-9.6598 (-1)	-3.7969 (-3)	+1.6134 (-1)	+6.1504 (-2)
0.10	+2.2080	-1.3725	-1.0084 (-1)	+5.2421 (-1)	+2.9689 (-1)
0.14	+2.0348	-1.4474	-1.6127 (-1)	+8.9285 (-1)	+5.8228 (-1)
0.18	+1.8685	-1.1680	+3.6891 (-3)	+1.0950	+6.9230 (-1)
0.22	+1.7122	-6.1943 (-1)	+3.7914 (-1)	+1.0840	+5.7395 (-1)
0.26	+1.5761	+4.0243 (-2)	+8.5064 (-1)	+8.7752 (-1)	+2.8419 (-1)
0.30	+1.4684	+6.9223 (-1)	+1.2813	+5.1912 (-1)	-8.8392 (-2)
0.34	+1.3803	+1.2509	+1.5727	+6.4764 (-2)	-4.6735 (-1)
0.38	+1.3027	+1.6598	+1.6851	-4.0421 (-1)	-7.7972 (-1)
0.42	+1.2288	+1.9048	+1.6251	-8.1187 (-1)	-9.7838 (-1)
0.46	+1.1542	+1.9984	+1.4391	-1.1114	-1.0570
0.50	+1.0783	+1.9742	+1.1833	-1.2913	-1.0341

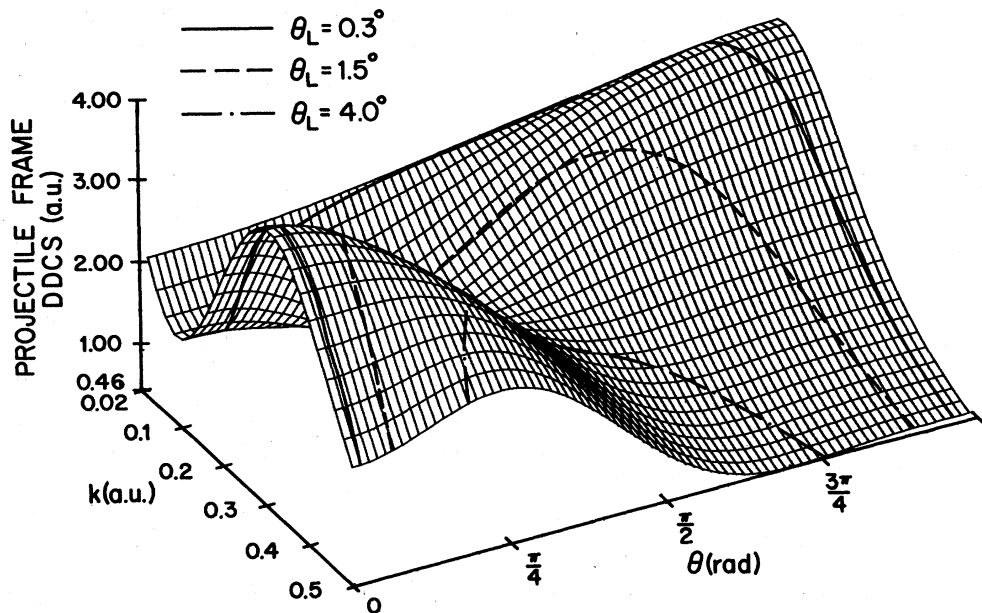


FIG. 1. Galilean-invariant, detachment doubly differential cross section (DDCS) in the projectile frame vs  $\mathbf{k}=(k,\theta)$ . The three trajectories on the surface map the Galilean-invariant cross sections in the laboratory frame as a function of electron momentum for three fixed laboratory angles for the detached electron (i.e.,  $\theta_L=0.3^\circ$ ,  $1.5^\circ$ , and  $4.0^\circ$ ). The results shown employ an effective excitation energy  $\bar{I}_{\text{He}}$  of 35 eV for the helium target.

tation energy  $\bar{I}_{\text{He}}$  of 35 eV for the helium target. We have computed similar results, shown elsewhere,<sup>23</sup> using a value of 21.2 eV for  $\bar{I}_{\text{He}}$ . Qualitatively, our two results have the same features as obtained by Maleki and Macek.<sup>9</sup> Namely, for  $k \approx 0$ , there is a large peak for  $\theta \approx \pi$  (i.e., for detached electrons traveling with the H atom); for  $k \approx 0.5$  there is a large peak for smaller angles  $\theta$  corresponding to the so-called binary encounter peak.<sup>15</sup> These two regimes are divided by a "valley" in the cross-section surface extending from  $(k \approx 0, \theta \approx 0)$  to  $(k \approx 0.5, \theta \approx 3\pi/4)$ . The origin of this valley is discussed below.

Quantitatively, our results are sensitive to the choice of  $\bar{I}_{\text{He}}$ . The cross sections obtained with use of the  $1s2p(^1P)$  value (i.e., 21.2 eV) for  $\bar{I}_{\text{He}}$  are considerably larger than those shown in Fig. 1, which were calculated using the value 35 eV (Ref. 12) obtained from the averaging procedure of Lee and Chen<sup>17</sup> for small scattering angles. Our results differ quantitatively also from those of Maleki and Macek<sup>9</sup> due primarily to our differing  $\text{H}^-$  wave functions, which include angular correlations, our differing value for  $\bar{I}_{\text{He}}$ , and our use of different values for the He atomic form factor and incoherent scattering function.

### B. Doubly differential detachment cross section in the laboratory frame

The trajectories drawn on the cross-section surface in Fig. 1 trace the laboratory-frame Galilean-invariant DDSCS as a function of electron momentum for the three fixed laboratory angles,  $\theta_L=0.3^\circ$ ,  $1.5^\circ$ , and  $4.0^\circ$ . Because of the valley in the projectile-frame DDSCS, one sees that these laboratory-frame trajectories have two maxima.

Two-dimensional plots of the ordinary laboratory-

frame DDSCS's [cf. Eqs. (12) and (34)] corresponding to these trajectories are shown as a function of laboratory-frame electron kinetic energy in Fig. 2 at four fixed detachment electron-scattering angles,  $\theta_L$ . One sees that the DDSCS decreases with increasing  $\theta_L$ . Furthermore, the double-peak structure disappears by  $\theta_L \gtrsim 4.0^\circ$ .

### C. Origin of the double-peak structure in the laboratory-frame DDSCS for small scattering angles

The valley in the projectile-frame DDSCS shown in Fig. 1 and the resulting double-peak structure for small angles in the laboratory-frame DDSCS shown in Fig. 2 stem from

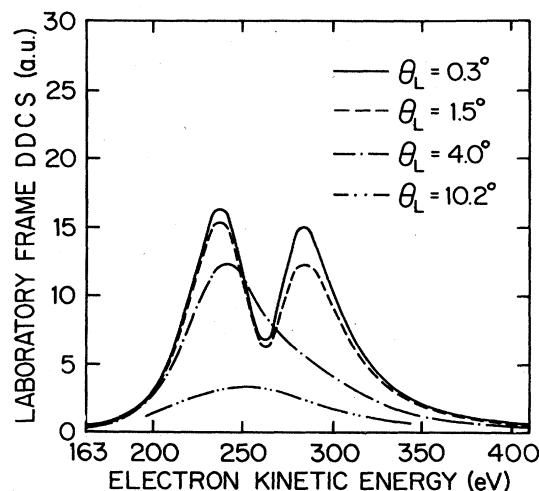


FIG. 2. Laboratory-frame DDSCS's vs electron kinetic energy for the four fixed detachment electron ejection angles,  $\theta_L=0.3^\circ$ ,  $1.5^\circ$ ,  $4.0^\circ$ , and  $10.2^\circ$ .

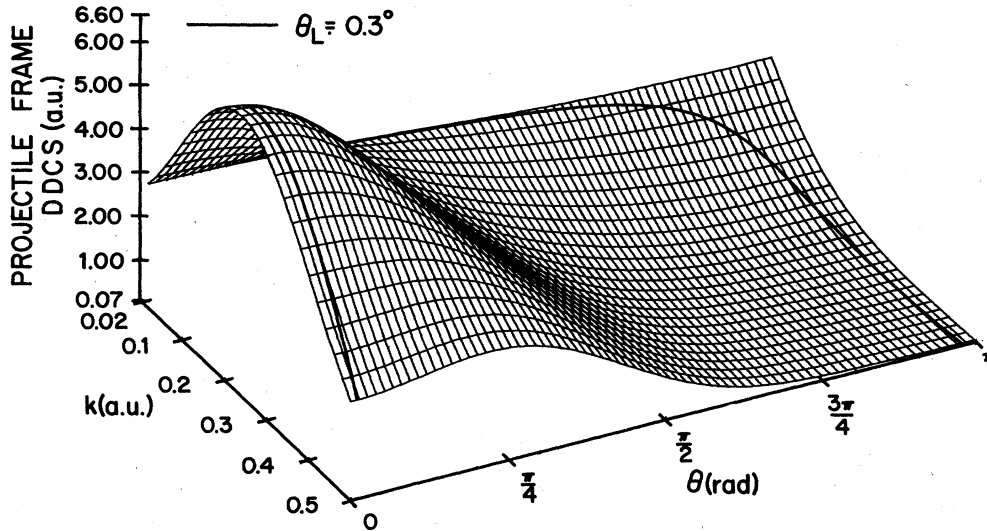


FIG. 3. Fictitious calculation in which the  $s$ -wave phase shift for the detached electron is fixed at 0 rad. All other data and the description are the same as in Fig. 1 except that only the  $\theta_L=0.3^\circ$  trajectory is shown.

an interference<sup>7</sup> of  $s$  and  $p$  partial-wave contributions to the DDCS. This interference may be seen analytically by examining the structure of  $J(K, \mathbf{k})$ , as done by Macek *et al.*<sup>5</sup> The function  $J(K, \mathbf{k})$  contributes to the DDCS as in Eq. (12). It is defined in Eq. (13) as the average over azimuthal angles of the absolute square of the  $H^-$  transition form factor. The interference is visible, however, only when the transition form factor is expanded in partial-wave components,  $Q_{\mu\mu'}^l(K, k)$ , as in Eqs. (29) and (30) and Eqs. (A1)–(A5) in the Appendix. From these latter equations we may write

$$J(K, \mathbf{k}) = (Q_{\mu\mu'}^0)^2 + (Q_{\mu\mu'}^1)^2 [1 - \xi^2 + (3\xi^2 - 1)\cos^2\theta] / 2 \\ + 2\xi \cos\theta Q_{\mu\mu'}^0 Q_{\mu\mu'}^1 \cos(\delta_1 - \delta_0) + \dots, \quad (35)$$

where we have left out terms involving partial-wave transition form factors with  $l \geq 2$ . The coefficient  $\xi$  depends on  $\bar{I}_{He}$  as in Eq. (A3). Thus, the larger the average target excitation energy, the more pronounced is the interference.<sup>5</sup> Cancellation occurs in Eq. (35) between the terms even and odd in  $\cos\theta$  for  $k \approx 0$ . For  $\delta_1 \approx \delta_0 \approx 0$  this cancellation occurs for  $\theta \approx \pi$ . In  $H^-$ , however, the  $s$ -wave phase shift  $\delta_0$ , is approximately equal to  $\pi$  for  $k=0$ . Hence the cancellation in Eq. (35) occurs near  $\theta \approx 0$  for  $k \approx 0$ , as shown in Fig. 1.

To demonstrate this explanation explicitly, we have carried out fictitious calculations using the same data as were used to compute the DDCS's in Figs. 1 and 2 (i.e., the same  $Q_{\mu\mu'}^l$  for  $0 \leq l \leq 2$ , the same  $\xi$ , and the same  $\delta_l$  for  $1 \leq l \leq 2$ ) but replacing the true  $s$ -wave electron phase shift  $\delta_0(k)$  by zero. The results for the projectile frame and the laboratory-frame DDCS are shown in Figs. 3 and 4. Figure 3 shows that there is no longer any valley; the cancellation which does occur is at  $\theta \approx \pi$ . The laboratory-frame DDCS at  $\theta_L = 0.3^\circ$ , which has the trajectory shown in Fig. 3, is shown in Fig. 4. One sees that in contrast to Fig. 2 there is only a single-peak structure. Hence we have demonstrated explicitly that the double-peak structure in the laboratory-frame DDCS is due to

the  $s$ -wave phase shift's value of  $\pi$  for slow detached electrons from  $H^-$  and to the resulting  $s$ - and  $p$ -wave interference.

More precisely, our calculation shows that interference of the  $s$  wave with the  $p$ - and  $d$ -wave terms is responsible for the valley in the cross-section surface in Fig. 1. However, Table I shows that the  $s$ - $p$  interference term  $C_1$  is much larger than the  $s$ - $d$  interference term  $C_2$  for small  $k$ . Thus, it is the  $s$ - $p$  interference which is primarily responsible for the valley. Note also that  $s$ - $d$  interference produces structure which is symmetric around  $\theta=90^\circ$ , whereas the valley in Fig. 1 is a decidedly asymmetric feature. Such asymmetric features can be caused only by  $s$  waves interfering with *odd* partial waves. We conclude, therefore, that the  $s$ - $p$  interference is responsible for the

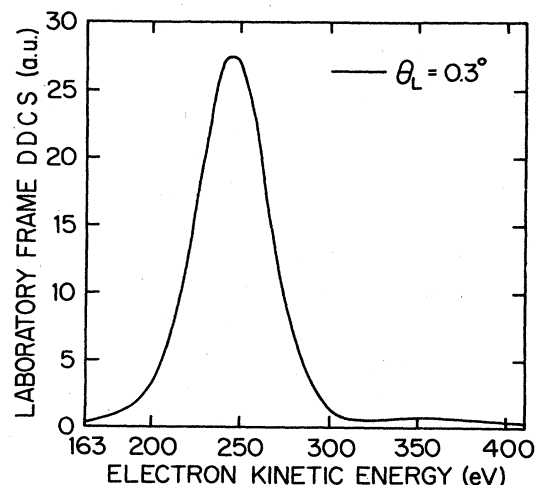


FIG. 4. Fictitious calculation in which the  $s$ -wave phase shift for the detached electron is fixed at 0 rad. All other data and the description are the same as in Fig. 2 except that only the  $\theta_L=0.3^\circ$  DDCS is shown.

valley in Fig. 1 and for the two peaks in the laboratory-frame results at small energies and angles.

#### D. Comparison with experimental results

Comparisons of our laboratory-frame DDCS's with the relative experimental measurements of Menendez and Duncan<sup>4,5</sup> are shown in Figs. 5 and 6. Our results in Fig. 5 employ an average He excitation energy  $\bar{I}_{\text{He}}$  of 35 eV while our results in Fig. 6 employ value of 21.2 eV. The experimental results have been normalized so that the lower-energy peak height agrees with our theoretical result.

Comparison of Figs. 5 and 6 shows that the energy positions of the DDCS peaks are predicted much more accurately using 35 eV for  $\bar{I}_{\text{He}}$ , according to the averaging procedure of Lee and Chen.<sup>17</sup> This averaging procedure provides an angle-dependent value of  $\bar{I}_{\text{He}}$ . We have simply chosen the value appropriate for small angles.<sup>12</sup>

The shapes of our predicted DDCS's are in excellent agreement with experiment for all angles  $\theta_L$  greater than

approximately  $4^\circ$ , for which there is only a single peak. For smaller angles, the predicted lower-energy peak agrees reasonably with experimental results, but the predicted higher-energy peak occurs higher in energy and is lower in magnitude than observed experimentally. As the only approximation we have made in our calculations which we feel might have a substantial effect on our results is the restriction of the H atom to the  $1s$  level, we feel that our results offer indirect proof of the importance of H-atom excitation states to the observed higher-energy peak. This conclusion is supported by the direct calculations (including excitation of H to the  $2s$  level) of Wright *et al.*<sup>12</sup> and the new experimental results of Duncan *et al.*<sup>6</sup> measured at and near  $\theta_L = 0^\circ$ .

The only absolute experimental data available are those for the single differential cross section (SDCS) for electron detachment.<sup>24</sup> These results are plotted as a function of electron ejection angle in the laboratory frame in Fig. 7. Also shown in Fig. 7 are four theoretical results: our present results employing the optimized (OP) and first optically excited state ( $^1P$ ) values for  $\bar{I}_{\text{He}}$  of 35 and 21.2 eV,

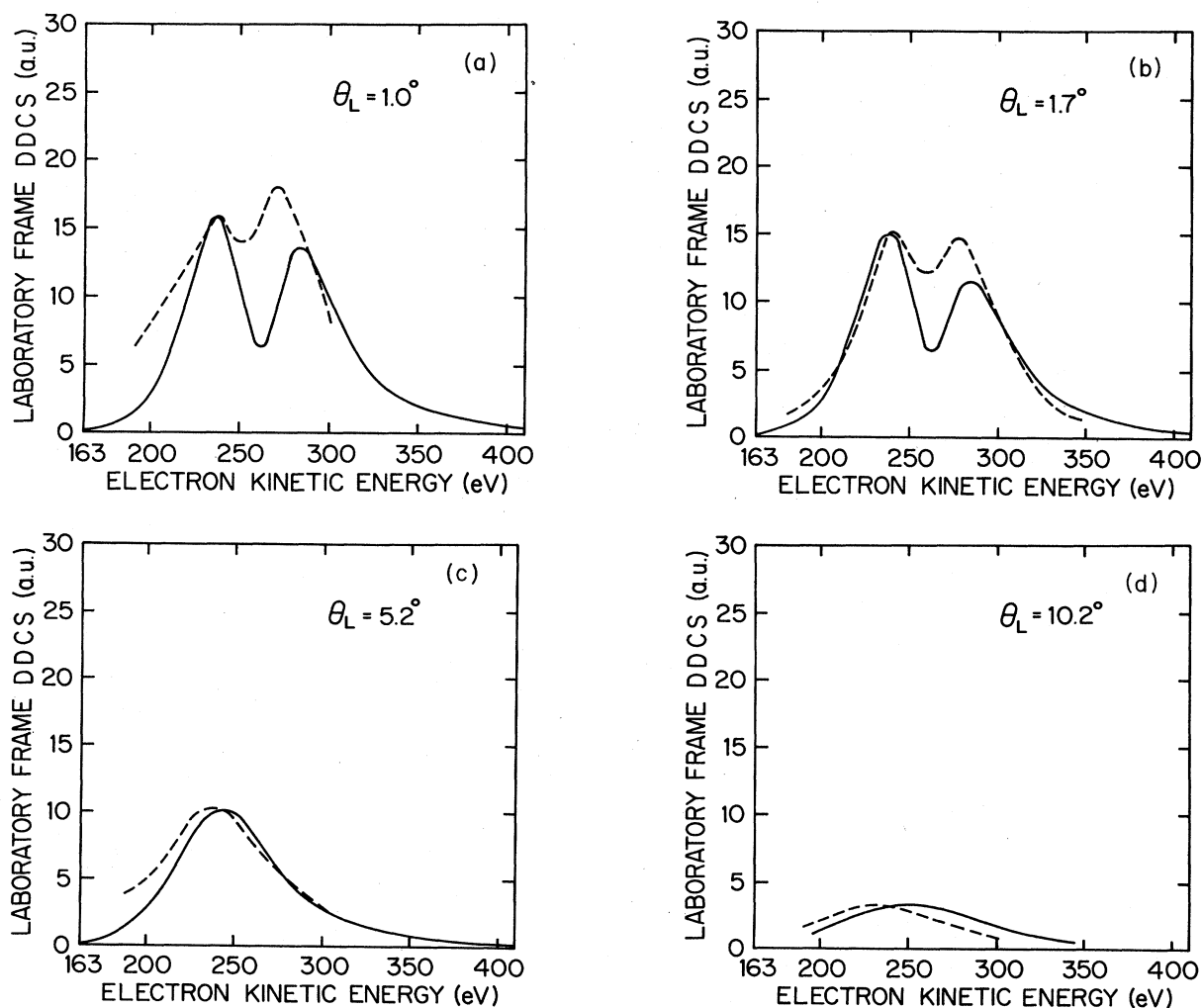


FIG. 5. Laboratory-frame DDCS's vs electron kinetic energy for the four fixed detachment electron ejection angles,  $\theta_L = 1.0^\circ$ ,  $1.7^\circ$ ,  $5.2^\circ$ , and  $10.2^\circ$ . Solid lines: present theoretical results employing  $\bar{I}_{\text{He}} = 35$  eV. Dashed lines: experimental results of Menendez and Duncan (Refs. 4 and 5). The experimental low-energy peak heights are normalized to our theoretical prediction.

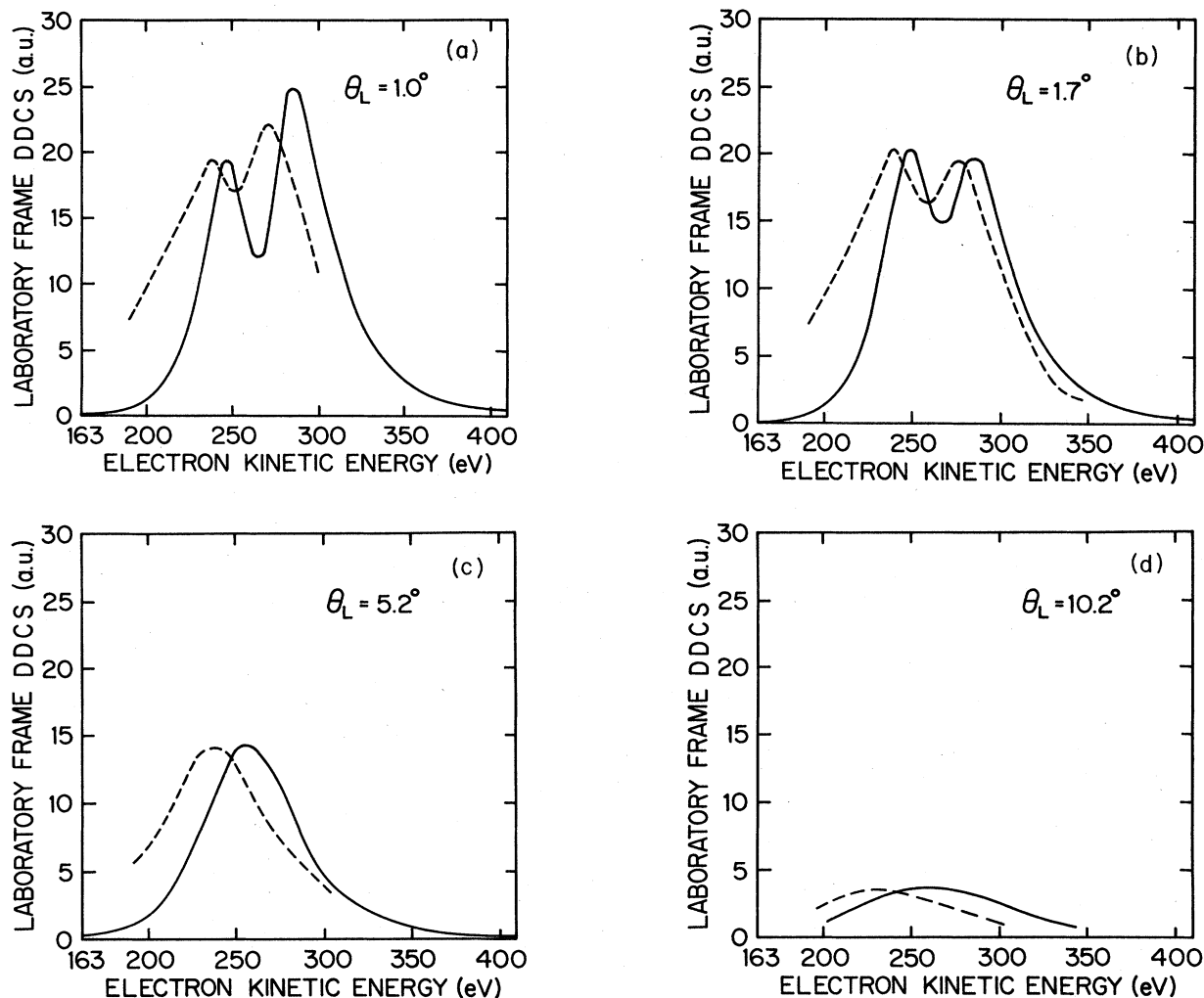


FIG. 6. Laboratory-frame DDCCS's vs electron kinetic energy for the four fixed detachment electron ejection angles,  $\theta_L = 1.0^\circ$ ,  $1.7^\circ$ ,  $5.2^\circ$ , and  $10.2^\circ$ . Solids lines: present theoretical results employing  $\bar{I}_{\text{He}} = 21.2$  eV. Dashed lines: experimental results of Menendez and Duncan (Refs. 4 and 5). The experimental low-energy peak heights are normalized to our theoretical prediction.

respectively; results of Macek *et al.*<sup>5</sup> using the techniques and approximations of Ref. 9; and electron-scattering-model (ESM) results of McCarthy *et al.*<sup>25</sup> on the SDCS of 300-eV electrons incident on He. One sees that our best results (OP) are lower than those of Macek *et al.* for  $\theta_L \leq 2^\circ$  and higher above  $2^\circ$ . Throughout the range  $0^\circ \leq \theta_L \leq 10^\circ$  our best results are about a factor of 2 higher than experiment. This discrepancy is at present not understood either theoretically or experimentally.<sup>26</sup>

## V. CONCLUSIONS

Our aim in this paper has been to present quantitatively accurate predictions for the dominant detachment process for  $\text{H}^-$  projectiles incident on He, namely, those in which the residual H atom is unexcited. Differences of our results in comparison with experiment thus serve as indirect evidence of the magnitude of contributions of excited H-atom states to the detachment cross section. In our calcu-

lations we have treated electron correlations within the  $\text{H}^-$  system more completely than have previous theoretical calculations. In particular, we have included angular correlations for the first time within the framework of an adiabatic hyperspherical coordinate treatment.<sup>13</sup> We have also used the most accurate estimate<sup>17</sup> for the average excitation energy of the He target as well as precise values<sup>16</sup> for the atomic form factor and incoherent scattering functions for He.

Our principal conclusions are, first, that the higher-energy peak observed experimentally has significant contributions from excited states of H, in agreement with the direct calculations of Wright *et al.*<sup>12</sup> We find that the positions and shapes of the peaks are predicted best when the description of Lee and Chen<sup>17</sup> for the average He excitation energy is used. Though our single differential cross sections differ quantitatively from previous calculations,<sup>9</sup> the factor of 2 discrepancy of the theoretical calculations with the absolute experimental data remains unexplained. Finally, we have performed fictitious calculations in

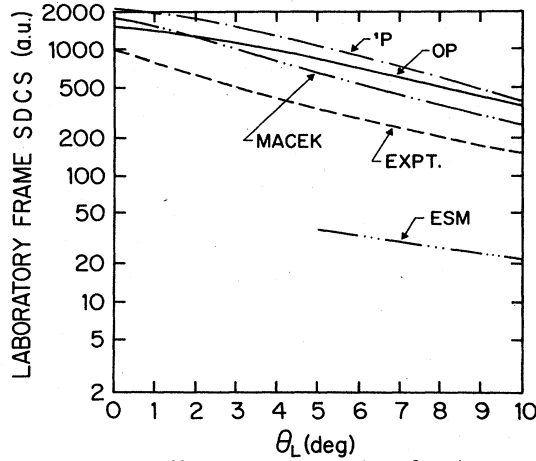


FIG. 7. Single differential cross sections for electron detachment vs detached electron-scattering angle. OP: present results employing the optimized value for  $\bar{I}_{\text{He}}$  of 35 eV.  $^1P$ : present results employing the  $1s2p(^1P)$  excitation energy for  $\bar{I}_{\text{He}}$  of 21.2 eV. MACEK: results of Macek *et al.* from Fig. 5 of Ref. 5. EXPT: experimental results of Menendez and Duncan from Fig. 5 of Ref. 5. ESM: electron-scattering results for 300-eV electrons on He of McCarthy *et al.* (Ref. 25) from Fig. 5 of Ref. 5.

which the  $s$ -wave phase shift is fixed at zero radians and have shown that the double-peak structure of the DDCS at small laboratory ejection angles disappears. We have thereby confirmed explicitly the origin of the double-peak structure as due, first, to the interference of  $s$  and  $p$  partial waves for the detached electron and, second, to the zero-energy  $s$ -wave phase shift of  $\pi$  degrees.

#### ACKNOWLEDGMENTS

We wish to thank Professor M. G. Menendez for providing us with his raw data and for several useful conversations. This work was supported in part by U.S. Department of Energy Contract No. DE-AC02-82ER12081.

#### APPENDIX

We provide here analytic expressions for the coefficients  $Z_n(K, k)$  defined in Eq. (33). We do this in two steps. First we obtain  $J(K, \mathbf{k})$  from its definition in Eq. (13) and from our approximate expression in Eq. (32) for the  $H^-$  transition form factor as follows:

$$J(K, \mathbf{k}) \equiv \sum_{n=0}^4 i_n T_n, \quad (\text{A1})$$

where

$$i_n \equiv \frac{1}{2\pi} \int_0^{2\pi} (\hat{\mathbf{K}} \cdot \hat{\mathbf{k}})^n d\phi_f. \quad (\text{A2})$$

The values for the integrals in Eq. (A2) may be expressed in terms of  $\cos\theta$  and a parameter  $\xi$ , where

$$\xi \equiv (2m_{\text{He}} \bar{I}_{\text{He}} + K^2) / (2k_i K), \quad (\text{A3})$$

as follows:

$$i_0 = 1, \quad (\text{A4a})$$

$$i_1 = \xi \cos\theta, \quad (\text{A4b})$$

$$2i_2 = (1 - \xi^2) + \cos^2\theta(3\xi^2 - 1), \quad (\text{A4c})$$

$$2i_3 = \cos\theta[3\xi(1 - \xi^2)] + \cos^3\theta(5\xi^3 - 3\xi), \quad (\text{A4d})$$

$$8i_4 = 3(1 - \xi^2)^2 + \cos^2\theta(-30\xi^4 + 36\xi^2 - 6) + \cos^4\theta(35\xi^4 - 30\xi^2 + 3). \quad (\text{A4e})$$

The coefficients  $T_n$  are given in terms of the coefficients  $Q_{\mu\mu'}^l$  and the detached electron's phase shifts,  $\delta_l$ , defining the  $H^-$  transition form factor in Eq. (32), in which only  $s$ ,  $p$ , and  $d$  partial-wave angular momenta  $l$  are kept:

$$T_0 = (Q_{\mu\mu'}^0)^2 + (Q_{\mu\mu'}^2)^2 / 4 - Q_{\mu\mu'}^0 Q_{\mu\mu'}^2 \cos(\delta_2 - \delta_0), \quad (\text{A5a})$$

$$T_1 = 2Q_{\mu\mu'}^0 Q_{\mu\mu'}^1 \cos(\delta_1 - \delta_0) - Q_{\mu\mu'}^1 Q_{\mu\mu'}^2 \cos(\delta_2 - \delta_1), \quad (\text{A5b})$$

$$T_2 = (Q_{\mu\mu'}^1)^2 - 3(Q_{\mu\mu'}^2)^2 / 2 + 3Q_{\mu\mu'}^0 Q_{\mu\mu'}^2 \cos(\delta_2 - \delta_0), \quad (\text{A5c})$$

$$T_3 = 3Q_{\mu\mu'}^1 Q_{\mu\mu'}^2 \cos(\delta_2 - \delta_1), \quad (\text{A5d})$$

$$T_4 = 9(Q_{\mu\mu'}^2)^2 / 4. \quad (\text{A5e})$$

Comparing the two expressions for  $J(K, \mathbf{k})$  in Eqs. (33) and (A1) and using the results in Eqs. (A4) and (A5), we have then for the desired coefficients  $Z_n(K, k)$  the following expressions:

$$Z_0 = T_0 + (1 - \xi^2)T_2 / 2 + 3(1 - \xi^2)T_4 / 8, \quad (\text{A6a})$$

$$Z_1 = \xi T_1 + 3\xi(1 - \xi^2)T_3 / 2, \quad (\text{A6b})$$

$$Z_2 = (3\xi^2 - 1)T_2 / 2 - (15\xi^4 + 18\xi^2 - 3)T_4 / 4, \quad (\text{A6c})$$

$$Z_3 = (5\xi^3 - 3\xi)T_3 / 2, \quad (\text{A6d})$$

$$Z_4 = (35\xi^4 - 30\xi^2 + 3)T_4 / 8. \quad (\text{A6e})$$

<sup>1</sup>M. E. Rudd and J. H. Macek, *Case Stud. At. Phys.* **3**, 47 (1972).

<sup>2</sup>F. Drepper and J. S. Briggs, *J. Phys. B* **9**, 2063 (1976).

<sup>3</sup>J. S. Risley, in *Electronic and Atomic Collisions*, edited by N. Oda and K. Takayanagi (North-Holland, Amsterdam, 1980), pp. 619–633.

<sup>4</sup>M. G. Menendez and M. M. Duncan, *Phys. Rev. A* **20**, 2327 (1979).

<sup>5</sup>J. Macek, M. G. Menendez, and M. M. Duncan, *Phys. Rev. A*

**29**, 516 (1984).

<sup>6</sup>M. M. Duncan, M. G. Menendez, and J. L. Hopkins, *Phys. Rev. A* **30**, 655 (1984).

<sup>7</sup>M. R. Frantz, L. A. Wright, and T. C. Genoni, *Phys. Rev. A* **24**, 1135 (1981).

<sup>8</sup>M. H. Day, *Phys. Rev. A* **26**, 1260 (1982).

<sup>9</sup>N. Maleki and J. Macek, *Phys. Rev. A* **26**, 3198 (1982).

<sup>10</sup>O. H. Crawford, *Bull. Am. Phys. Soc.* **29**, 777 (1984).

<sup>11</sup>A. L. Orbeli, E. P. Andreev, V. A. Ankudinov, and V. M.

- Dukel'skii, Zh. Eksp. Teor. Fiz. 58, 1938 (1970) [Sov. Phys.—JETP 31, 1044 (1970)].
- <sup>12</sup>L. A. Wright, T. C. Genoni, and M. R. Franz, Bull. Am. Phys. Soc. 28, 799 (1983).
- <sup>13</sup>J. Macek, J. Phys. B 1, 831 (1968).
- <sup>14</sup>C. L. Pekeris, Phys. Rev. 126, 1470 (1962).
- <sup>15</sup>J. S. Briggs and K. Taulbjerg, in *Structure and Collisions of Ions and Atoms*, Vol. 5 of *Topics in Current Physics*, edited by I. A. Sellin (Springer, Berlin, 1978), pp. 105–153.
- <sup>16</sup>J. H. Hubbell, W. J. Veigele, E. A. Briggs, R. T. Brown, D. T. Cromer, and R. J. Howerton, J. Phys. Chem. Ref. Data 4, 471 (1975).
- <sup>17</sup>Y. T. Lee and J. C. Y. Chen, Phys. Rev. A 19, 526 (1979).
- <sup>18</sup>N. F. Mott and H. S. W. Massey, *The Theory of Atomic Collisions*, 3rd ed. (Oxford University, London, 1971), Chaps. XII, Sec. 3 and XVI, Sec. 7.
- <sup>19</sup>H. A. Bethe, Ann. Phys. (Leipzig) 5, 325 (1930).
- <sup>20</sup>Reference 18, p. 477.
- <sup>21</sup>See, e.g., A. F. Starace, in *Handbuch der Physik, Vol. 31*, edited by W. Mehlhorn (Springer, Berlin, 1982), pp. 1–121, especially Sec. 4.
- <sup>22</sup>A. F. Starace and G. L. Webster, Phys. Rev. A 19, 1629 (1979), Appendix.
- <sup>23</sup>Chang-Hwan Park, Ph.D. thesis, The University of Nebraska, 1984.
- <sup>24</sup>See Fig. 4 of Ref. 4 and Fig. 5 of Ref. 5.
- <sup>25</sup>I. E. McCarthy, C. J. Noble, B. A. Phillips, and A. D. Turnbull, Phys. Rev. A 15, 2173 (1977).
- <sup>26</sup>M. G. Menendez (private communication).